# Photochemical & Photobiological Sciences

Accepted Manuscript


This is an *Accepted Manuscript*, which has been through the Royal Society of Chemistry peer review process and has been accepted for publication.

*Accepted Manuscripts* are published online shortly after acceptance, before technical editing, formatting and proof reading. Using this free service, authors can make their results available to the community, in citable form, before we publish the edited article. We will replace this *Accepted Manuscript* with the edited and formatted *Advance Article* as soon as it is available.

You can find more information about *Accepted Manuscripts* in the Information for Authors.

Please note that technical editing may introduce minor changes to the text and/or graphics, which may alter content. The journal's standard Terms & Conditions and the Ethical guidelines still apply. In no event shall the Royal Society of Chemistry be held responsible for any errors or omissions in this *Accepted Manuscript* or any consequences arising from the use of any information it contains.

ROYAL SOCIETY OF CHEMISTRY

www.rsc.org/pps

# Pigment Violet 19 – a Test Case to Define a Simple Method to Simulate the Vibronic Structure of Absorption Spectra of Organic Pigments and Dyes in Solution

Benoît CHAMPAGNE, Vincent LIÉGEOIS, and Freddy ZUTTERMAN

*Laboratoire de Chimie Théorique, Unité de Chimie-Physique Théorique et Structurale, Université de Namur, rue de Bruxelles, 61, B-5000 Namur (BELGIUM).*

**Abstract**

A typical quinacridone pigment, PV19, has been used to analyze the impact of several computational parameters on the UV/vis absorption band shape in solution, simulated using density functional theory and time-dependent density functional theory levels of approximation. These encompass, i) the choice of exchange-correlation functional, ii) the basis set, iii) the method for non-equilibrium optimization of the excited state geometry, iv) the approach for evaluating the vibronic band structure, v) the peak broadening, and vi) the scaling of the harmonic vibrational frequencies. Among these, the choice of exchange-correlation functional is certainly of the most importance because it can drastically modify the spectral shape. In the case of PV19, the M05-2X and to a lesser extent CAM-B3LYP XC functionals are the most efficient to reproduce the vibronic structure, confirming the important role of exact Hartree-Fock exchange. Still, these functionals are not the most reliable to predict the excitation energies and oscillator strengths, for which M05, a functional with less HF exchange, performs better. For evaluating the vibronic structure, the simple gradient method, where only one step of geometry optimization of the excited state is carried out and the gradients are used to evaluate the Huang-Rhys factors as well as to determine the excited state geometries produces a spectrum that is very similar to the ones obtained with the more involved Duschinsky and geometry methods, opening the way to a fast simulation of the UV/vis absorption spectra of pigments and dyes. Then, the effect of scaling the calculated vibrational frequencies to account for anharmonicity effects as well as for limitation of the method also impacts the shape of the vibronic spectrum and this effect depends on the method used to determine the Huang-Rhys factors. Indeed, scaling the vibrational frequencies by a factor which is typically smaller than 1.0 results in a relative decrease of the 0-1 peak intensity with respect to the 0-0 band when optimizing the geometry of the excited state whereas the effect is opposite and magnified if using the gradient method.

## I. Introduction

Designing organic compounds and materials with targeted colors remains a challenge with important technological applications.[1] Besides scattering effects, color is determined by the absorption spectrum of the compounds, which goes beyond listing the wavelengths corresponding to the absorption band maxima. Indeed, color is also determined by the intensities as well as by the shapes of the different absorption bands in the visible wavelength range. The complex process to design colored materials can take advantage of structure-color relationships, derived over many decades using spectroscopic characterizations.[2] More recently, owing to the access to computational facilities of increasing power, theoretical chemistry has appeared as a complementary tool.[3-6] Still, the prediction of the color of a given material relies on the accurate prediction of the optical properties of the constitutive molecules as well as of the impact of its surrounding in the material.

Quinacridones represent a major family of industrially important pigments. While quinacridones are most often used as solid pigment dispersions in practical applications, the understanding of the spectrum of the non-aggregated molecule, as investigated here, is a crucial first step in understanding the absorption spectrum of the solid pigment. Inter-molecular coupling effects that modify the absorption spectrum in the solid state have been modeled at various levels of approximation for quinacridones.[7]

This paper addresses the first step of these color prediction and design by reporting on the use of quantum chemistry methods to predict the absorption band shape in solution of a typical quinacridone pigment, Pigment Violet 19 (PV19). PV19 is the structurally simplest representative of this family of industrially important pigments. Though high-level *ab initio* methods have been designed to predict molecular optical properties,[4] these theoretical simulations are usually based on the methods of the time-dependent density functional theory (TDDFT),[5-6] which can be employed to large systems in limited computational time. Besides the choice of exchange-correlation (XC) functional, several technical aspects of predicting the vibronic band structure are assessed in comparison with the experimental spectrum. Next Section describes the different methodological and computational aspects of these simulations while the results are presented and discussed in Section 3. Section 4 draws the main conclusions of this paper.

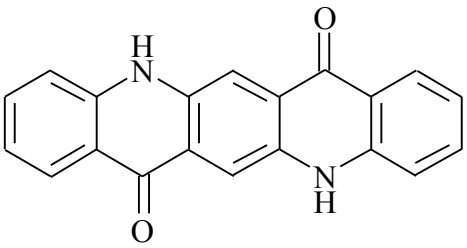


**Scheme 1**: Sketch of the PV19 molecule

## II. Methodological and computational aspects

### *II.A. Ground state geometries and exchange-correlation functionals*

The molecular geometry of the PV19 ground state in solvent was optimized using DFT, followed by a calculation of the vibrational frequencies to confirm it is stationary point on the potential energy surface. The 6-31G(d) basis set was used in most cases while additional calculations were performed with the 6-311G(d), 6-31G(d,p), and 6-31+G(d) basis sets to assess the impact of adding a set of valence, polarization on the H atoms, and diffuse functions, respectively. Solvent (DMSO) effects were taken into account with the IEF-PCM method.[8] The following exchange-correlation functionals were used: B3LYP-35,[9] Gaussian version of BHandHLYP,[10] M05,[11] M05-2X,[11] LC-BLYP,[12] and CAM-B3LYP.[13] BHandHLYP is a hybrid GGA functional, where the GGA correlation is provided by the LYP expression and the exchange part is a mixture of the GGA (Becke) exchange functional with 50% of HF exchange.[10] B3LYP-35 is a modified version of B3LYP,[14] having 35 % exact HF exchange instead of the standard 20 %, that was employed successfully in previous works on the vibronic structure and resonant Raman spectra of julolidinemalononitrile.[9] M05 and M05-2X are hybrid meta-GGA functionals, which depend explicitly on the local kinetic energy density in the exchange-correlation potential, together with a part of HF exchange, which amounts to 28% and 56%, respectively.[11] Range-separated GGA hybrids were also considered with i) the LC-BLYP functional, which applies the long-range correction (LC) of Hirao and coworkers to BLYP, *i.e.* containing 100% of HF exchange at long range with a range-separating parameter ($\mu$) of 0.47,[12] and ii) the CAM-B3LYP functional, which adds a long-range correction using the Coulomb-attenuating method and includes 19% of HF exchange at short range and 65% at long range with $\mu$ = 0.33.[13] Comparisons of the results obtained with the hybrid functionals M05, B3LYP-35, BHandHLYP and M05-2X allow the assessment of the impact of varying the amount of range-independent exact HF exchange in the functional whereas their comparison with CAM-B3LYP and LC-BLYP informs about the impact of short- and long-range HF exchange. The latter two functionals are also expected to produce better results for relatively large molecules. In a few calculations the more recent M06-2X functional[15] (having 54 % HF exchange) was used, but this functional was not studied in much detail, since the results obtained were very similar to the ones obtained with M05-2X. All calculations were run with Gaussian 09 revision C.01.[16]

### *II.B. Excitation energy and geometry optimization of the excited states*

The excitation energies and transition dipoles for the 20 lowest-energy excited states were calculated at the TDDFT level.[17] The same functionals, basis sets, and solvation method were employed as for the ground state characterizations. For all excited state calculations an ultrafine integration grid was specified mainly because a small number of geometry optimizations of excited states failed to terminate when the default integration grid was used.

The excited states responsible for absorption of PV19 in the optical domain were identified. With all combinations of functional and basis set there was only one excited state with significant oscillator strength in the optical and "near"-optical domain, and this was always the first excited state.

The geometry of that relevant excited state was then optimized with TDDFT, using the same level of approximation.[18] A non-equilibrium solvation model was employed to describe the fast electronic process of optical absorption,[19] though this sometimes remains a non systematic approach.[6d] Indeed, the non-equilibrium solvation model allows the determination of the PV19 excited state geometry in equilibrium with the electronic degrees of freedom of the solvent, contrary to the situation where the electronic and orientational degrees of freedom of the solvent are fully relaxed relative to the electrostatic potential of the excited state. Two different methods were used to establish non-equilibrium solvation. In the first method we specify non-equilibrium solvation by using standard Gaussian keywords, which initiates a TDDFT excitation energy calculation, followed by geometry optimization of the first excited state with non-equilibrium solvation.[18b] This approach is here referred to as the "*td method*", owing to the `td = noneqsolv` Gaussian keyword. We also tried a second method for non-equilibrium solvation, where we specify an equilibrium solvation, but the static dielectric constant (which is the one used for full equilibrium solvation) is replaced by the dynamic dielectric constant, effectively causing only the electronic degrees of freedom of the solvent to adapt to the modified electron density of the excited state. In the case of DMSO, the optical dielectric constant is fixed at 2.007899. This second method of non-equilibrium solvation, which was employed in some of our recent investigations, is here called the "*eps method*".

An alternative to full geometry optimization of the excited state consists in calculating the gradients of the excited state energy with respect to the vibrational normal mode coordinates ($Q_\ell$) of the ground state. In that scheme, the $\Delta_\ell$ displacement along the normal coordinate $Q_\ell$ is given by the partial derivatives of the excited state electronic energy $E_e$ with respect to the normal coordinate $Q_\ell$ calculated at the ground state equilibrium geometry:

$$\Delta_\ell = -\frac{1}{\sqrt{\hbar\omega_\ell^3}}\left(\frac{\partial E_e}{\partial Q_\ell}\right)_0 \qquad (1)$$

That approach is very useful for difficult cases where the geometry optimization of the excited state fails, making it impossible to carry out the subsequent steps of the simulation of the spectrum on the basis of the optimized geometry of the excited state.

The vibrational frequencies and normal modes of the excited state were also determined using the procedure implemented in Gaussian 09,[18b] after performing geometry optimization with the "td method" or the "eps method".

### *II.C. Simulation of the absorption spectra*

Several approaches have been used to simulate the absorption spectrum and its vibronic structure. Once a functional, basis set, and a method for non-equilibrium solvation of the excited state has been chosen, the spectrum can be calculated at three different levels of "completeness" :

- Calculation of the spectrum with inclusion of the effects of Duschinsky rotation[20-21] represents the most complete procedure. In addition to the calculation of the ground state vibrational frequencies, calculation of the excited state vibrational frequencies is also required, which is the most time-consuming step in the procedure. However, this is the "reference" method against which simpler and faster methods need to be benchmarked. This procedure will be called the "duschinsky" procedure. It is feasible only if the optimized geometry of the excited state is not too different from the ground state geometry. This calculation is performed using the Gaussian code, which calculates recursively the Franck-Condon factors following Ref. 21b.
- A first approximation consists in ignoring Duschinsky rotation. This is a significantly faster procedure since it does not require the vibrational frequencies of the excited state to be calculated. Therefore, the assumption that the frequencies of the excited state are identical to the ones of the ground state is made. It will be called the "geometry" procedure. Like the "duschinsky" procedure, the "geometry" procedure fails if excited and ground state geometries are too different.
- In a further approximation, the geometry of the excited state is not optimized, and only the gradients in the excited state are calculated. Again, one assumes that the frequencies of the excited state are identical to the ones of the ground state. Since this corresponds to performing only one cycle of geometry optimization of the excited state, this is by far the fastest procedure. It will be called the "gradient" procedure. It is generally feasible, i.e. even if the optimized ground and excited state geometries are very different.

The "duschinsky" procedure is based entirely on the Gaussian09 package. In absence of Duschinsky rotation, however, an in-house-developed code was preferred because it allows using both the "geometry" and the "gradient" procedures. All procedures assume that the Born-Oppenheimer approximation is valid and that the potential energy surfaces of both the ground and excited states are harmonic. In the latter approach, the Franck-Condon overlap integrals are evaluated from the Huang-Rhys factors, $HR_\ell = \Delta_\ell^2 / 2$. Reliable results require that the sum of the Franck Condon factors be at least 0.95. To accelerate the convergence of these vibrational overlap calculations, the in-house procedure allows i) to eliminate all modes with a Huang-Rhys factor smaller than a threshold (set at $10^{-6}$ in this study), ii) to keep only the vibrational excitations with Franck-Condon factor larger than a threshold (set at $10^{-6}$ in this study), iii) to specify a limit on the maximum number of simultaneously excited modes (6 in this study), iv) to limit the maximum number of quanta in a vibrational normal mode (the

maximum number of quanta is not set the same in all modes but is automatically tuned as a function of the Huang-Rhys factors), and v) to eliminate troublesome vibrational normal modes from the Franck-Condon overlap calculations (typically, some modes with very low vibrational frequencies and large Huang-Rhys factors, however this was not necessary in the case of PV19). While the criterion on the sum of the Franck Condon factors is sufficient to know if all the important vibrational excitations have been taken into account, the program can show the individual errors made by using a specific threshold when keeping the important contributions (point ii), by the limit on the maximum number of simultaneously excited modes (point iii), and by the limit on the maximum number of vibrational quanta (point iv).

Several additional variables can be specified in the calculation of the spectra. Firstly, peak broadening needs to be applied to all vibronic transitions. Gaussian peak shapes were used with a typical full width at half of the maximum (FWHM) of 0.1 eV. Peak broadening is needed in order to empirically account for several factors which cannot be included in the theoretical treatment, e.g. inhomogeneous broadening because of different solvent configurations around the chromophore, Doppler effect, population of excited low-energy vibrational levels in the ground state. It is also needed in order to take account of peak broadening by coupling of the electronic excitation to low-energy vibrations (not necessary in the case of PV19) and rotations that cannot be included in the calculations (see above). However, it should be realized that replacing the true coupling to a low-energy vibrational mode with a large Huang-Rhys factor by peak broadening does not really produce the same effect. Indeed, while the coupling to the low-energy mode causes a shift of the peak maximum to lower energy together with a broadening, the empirical broadening does not shift the peak maximum. In addition, the Gaussian shape of the broadening differs from the Poisson distribution of the vibronic transitions. Still, in the case of PV19 none of the low-energy vibrations had to be excluded.

Moreover since the (TD)DFT calculated vibrational harmonic frequencies overestimate the experimental vibrational transition frequencies, it may be necessary to scale them by some factors.[22] These overestimations and thereof best scaling factors depend on the exchange-correlation functional. In the initial calculations no frequency scaling was applied, but the effect of this variable was investigated.

Finally, since the main purpose of this work is to compare absorption band shapes between different methods as well as between simulations and experiment, the spectrum can be shifted. Unless otherwise stated, the energy shift was selected such as to shift the maximum of the longest-wavelength absorption band (the "0-0" band for PV19) to exactly 523 nm (i.e. the experimental absorption maximum). Note that the true lowest-energy excitation in a vibronic structure is the true 0-0 excitation.

Summarizing, the impact of the following parameters on the calculated absorption band shape of PV19 is discussed in this paper :

- the exchange-correlation functional
- the basis set
- the method for non-equilibrium geometry optimization of the excited state geometry ("td" versus "eps")
- the method for calculation of the energies and oscillator strengths of the vibronic excitations ("duschinsky" vs "geometry" vs "gradient")
- the peak broadening
- the vibrational frequency scaling

The absorbance is calculated at energies spaced by a 0.001 eV interval, corresponding to a resolution of 0.22 nm at the experimental absorption maximum. This resolution, needed to allow detailed comparisons between different simulated spectra, is far better than the resolution of the experimental spectrum (1 nm).

### *II.D. Experimental method*

The experimental absorption spectrum was obtained by dissolving PV19 in DMSO at a concentration of 6.40 x $10^{-5}$ mole/liter. Absorbance was recorded at 1 nm intervals. The oscillator strength was calculated by integrating over the entire absorption band (from 400 to 550 nm) after plotting the spectrum as the molar extinction coefficient against the wave number (in $cm^{-1}$) :

$$f = 4.319 \times 10^{-9} \int \varepsilon\left(\tilde{\nu}\right) d\tilde{\nu} \qquad (2)$$

## III. Results and discussion

### *III.A. Effects of the XC functional on the vertical excitation and emission energies*

The equilibrium structure of PV19 in the ground state is perfectly planar, as determined with all functionals. Only the 1st excited state is responsible for absorption in the optical domain, since only this state has appreciable oscillator strength in or near optical frequencies. Resonance wavelengths and oscillator strengths for the vertical excitation from the equilibrium ground state geometry are compared to experimental data in Table 1. The experimental excitation energy corresponds to the maximum of absorption. This excited state is dominated by a HOMO to LUMO transition.

| | Vertical (nm) | Vertical (eV) | Oscillator strength | HOMO-LUMO Character (%) |
|---|---|---|---|---|
| M05 | 443 | 2.796 | 0.108 | 98.6 |
| B3LYP-35 | 421 | 2.942 | 0.129 | 98.3 |
| CAM-B3LYP | 397 | 3.127 | 0.158 | 95.8 |
| M05-2X | 394 | 3.144 | 0.161 | 96.9 |
| BHandHLYP | 384 | 3.230 | 0.164 | 96.9 |
| LC-BLYP | 348 | 3.568 | 0.217 | 90.0 |
| Experiment | 523 | 2.371 | 0.111 | |

**Table 1**. Vertical excitation energies and wavelengths as well as oscillator strengths as determined with different XC functionals in comparison to experiment. The calculations were performed on the corresponding ground state geometries by accounting for the solvent effects (DMSO) with the IEF-PCM scheme and using the 6-31G(d) basis set.

The following conclusions can be drawn from these data. The resonance is predicted at too short a wavelength with all functionals. The functional with the lowest % HF exchange (M05) gives a result that comes closest to the experimental value. Consequently, the excitation energy is quite strongly overestimated with all functionals. Even with the "best" functional the deviation is still 0.43 eV. A small part of this overestimation can be attributed to the atomic basis set as found by comparing the M05-2X vertical excitation energies calculated with the 6-31G(d), 6-311G(d), 6-31+G(d), and 6-31G(d,p) basis sets, which amounts to 3.144 eV, 3.080 eV, 3.017 eV, and 3.148 eV, respectively. However, this direct comparison between the maximum of the absorption band and the vertical excitation energy makes limited sense, since it does not take account of the vibronic structure (*vide supra*). The resonance wavelength decreases (i.e. the excitation energy increases) with increasing the percentage of HF exchange. This is in agreement with the behavior of TDDFT reported in the literature for other molecules.[5b] However, there is an inversion between BHandHLYP and M05-2X (which have similar percentages of HF exchanges). The highest excitation energy is obtained with the range-corrected functional LC-BLYP. CAM-B3LYP gives results quite comparable to results with M05-2X or BHandHLYP. The predicted oscillator strength corresponds well to the experimental value when functionals with a small percentage of HF exchange are used, and increases with the amount of HF exchange. This increase of oscillator strength with increasing amount of HF exchange is in agreement with the behavior of TDDFT reported for other molecules in the literature.[4a, 23]

The geometry optimization of the 1st excited state produced also a planar structure with all functionals, both with the "td" and "eps" method (bond length data are provided in section III.D). At that geometry, the vertical emission energies and oscillator strengths

calculated with the different XC functionals are listed in Table 2. As expected, the vertical emission energies are smaller than the excitation energies and the difference attains 0.21 – 0.28 eV (functionals M05 to M05-2X) and up to 0.40 eV with the LC-BLYP functional, which probably gives unrealistic results, as will be shown below. The change of the oscillator strengths with respect to absorption is very small, generally a reduction but smaller than 10% while the dominant character is still represented by a HOMO-LUMO transition. Moreover, the topology of these MO's does not change from the ground to the excited state geometries.

| | Vertical (eV) | Oscillator strength | HOMO-LUMO character (%) |
|---|---|---|---|
| M05 | 2.590 | 0.102 | 98.8 |
| B3LYP-35 | 2.704 | 0.122 | 98.8 |
| CAM-B3LYP | 2.847 | 0.147 | 96.9 |
| M05-2X | 2.863 | 0.150 | 97.7 |
| BHandHLYP | 2.928 | 0.154 | 97.4 |
| LC-BLYP | 3.161 | 0.196 | 91.9 |

**Table 2**. Vertical emission energies and oscillator strengths as determined with different XC functionals. The calculations were performed on the corresponding "td" optimized excited state geometries by accounting for the solvent effects (DMSO) with the IEF-PCM scheme and using the 6-31G(d) basis set.

### *III.B. Adiabatic and 0-0 excitation energies versus energies of maximum absorption*

The vibronic structure of the absorption spectrum was then calculated with the variety of methods and parameters described in section II.C. Details about the absorption band shape, and how well it matches with the experimental one, are given in the next Section. The predicted absorption maxima that were obtained by inclusion of the vibronic structure are given here, in order to compare them with the vertical resonance, adiabatic, and 0-0 excitation energies. The adiabatic excitation energy is the difference between the electronic energies of the two states at their respective equilibrium geometries. It lays in-between the vertical excitation and emission energies. The 0-0 excitation energy is the difference between the energies with zero-point contributions of the two states at their respective equilibrium geometries. It is slightly lower than the adiabatic excitation energy. Since this requires calculating the vibrational normal mode frequencies for both the ground and excited states, the data in Table 3 were obtained by using the Gaussian package, including Duschinsky rotation effects. The "td" excited state geometries were used and no frequency scaling was applied. For the determination of the maximum of absorption, the spectra have then been simulated using a FWHM of 0.1 eV while no spectral shift was applied. These predicted energies of maximum absorption, using the Duschinsky approach, are typically 0.015-0.025 eV larger than the 0-0 energies.

| | Vertical (GS) eV | Adiabatic (eV) | 0-0 (eV) | Abs max (eV) |
|---|---|---|---|---|
| M05 | 2.796 | 2.693 | 2.614 | 2.629 |
| B3LYP-35 | 2.942 | 2.824 | 2.752 | 2.769 |
| CAM-B3LYP | 3.127 | 2.989 | 2.921 | 2.939 |
| M05-2X | 3.144 | 3.006 | 2.933 | 2.954 |
| BHandHLYP | 3.230 | 3.081 | 3.016 | 3.036 |
| LC-BLYP | 3.568 | 3.369 | 3.312 | 3.337 |
| Experiment | | | | 2.371 |

**Table 3**. Different types of excitation energies as determined with different XC functionals in comparison to experiment. The calculations were performed using the corresponding ground and excited state geometries by accounting for the solvent effects (DMSO) with the IEF-PCM scheme and using the 6-31G(d) basis set. .

Several observations can be made. When the vibronic structure is taken into account the error between calculation and experiment is significantly reduced. M05 still gives the result that best matches the experimental data. With inclusion of the vibrational effects the absorption maximum gets closer to the experimental value by 0.17 eV (29 nm). The difference between the vertical excitation energy and the maximum of the calculated absorption band ranges from 0.17 eV (M05) to 0.23 eV (LC-BLYP). The position of the vertical excitation in the absorption band is illustrated in Fig. 1, using data obtained with B3LYP-35. The vertical excitation appears near the maximum of the "0-1" band, rather than near the absorption maximum. This illustrates the fact that comparing calculated vertical excitation energies (i.e. without taking account of the vibronic structure) with experimental absorption maxima makes limited sense. Obviously, the only parameter that can be directly compared with an experimental absorption maximum is the calculated absorption maximum, taking account of the vibrational effects. Despite this, comparisons between calculated vertical excitation energies and experimental absorption maxima are very frequently made in studies published in the literature, e.g. in order to assess the relative performance of many QM methods for predicting excitation energies. In the case of PV19, the absorption maximum is closer to the true 0-0 excitation than to the vertical excitation. This is typically the case when the geometry difference between the ground and excited state geometries is rather small, so that the "0-0" band has the highest intensity.

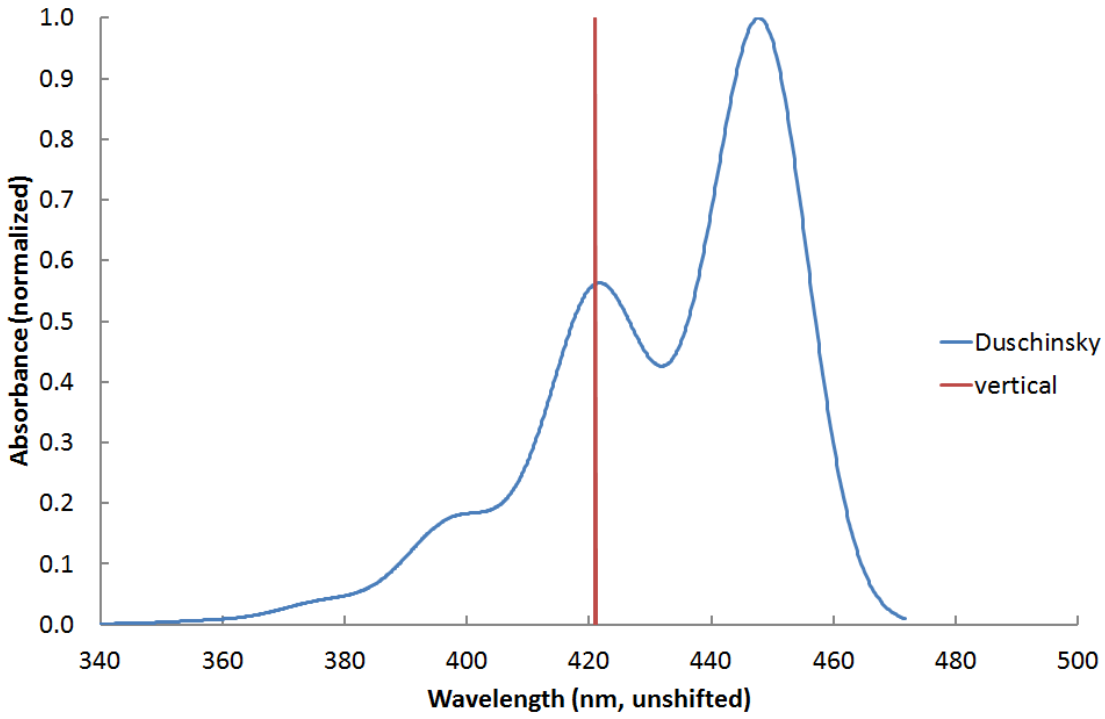


**Figure 1**. Visible absorption spectrum of PV19 as obtained with the TDDFT/B3LYP-35/6-31G(d) method and IEFPCM (solvent = DMSO) in comparison with the vertical excitation energy determined at the same level of approximation. The geometries and vibrational normal modes of both the ground and excited states were determined, and Duschinsky rotations were accounted for. The "td" non-equilibrium method was used and a 0.1 eV FWHM peak broadening was applied.

### *III.C. Vibronic structure*

This section concentrates in more detail on how well the experimental absorption band shape is reproduced by the various methods, and on the impact of the various simulation parameters on the band shape. A first interesting comparison (Fig. 2) shows the degree of variation obtained by choosing different functionals, illustrated with the spectra obtained with the "td" optimized excited state geometries and the "geometry" method. Calculated spectra are compared with the experimental spectrum. All simulated spectra have been displaced in such a way that the experimental and simulated absorption maxima coincide, which allows an efficient comparison between the shapes of the absorption bands.

The following conclusions can be drawn. When considering the intensity of the first vibrational satellite ("0-1 band") relative to the main ("0-0") band, the best match with the experimental spectrum is obtained when M05-2X is used. CAM-B3LYP also produces a reasonably good match. The two functionals with a low percentage of HF exchange (M05 and B3LYP-35) produce vibrational effects of too low intensity, showing that the geometry difference between the ground and excited states is underestimated. LC-BLYP, on the other hand, produces a far too large geometry difference, resulting in far too high intensity of the vibrational effects. Within the set of simple hybrid functionals without long-range correction

we observe an increase of the intensity of the vibrational effects with increasing the percentage of HF exchange, indicating an increasing geometry difference between the two states. This is illustrated by the values of the RMS displacements of the bond lengths between non hydrogen atoms of the excited state relative to the ground state structure, which amount to 0.054 Å, 0.059 Å, 0.066 Å, 0.069 Å, 0.069 Å, and 0.086 Å for the M05, B3LYP35, M05-2X, CAM-B3LYP, BHandHLYP, and LC-BLYP functionals, respectively. Moreover, as shown in Fig. 3, there is a quasilinear relationship between this RMS bond length displacement and the relative intensity of the 0-1 band relative to the 0-0 band.

The FWHM used (0.10 eV) seems to be quite adequate. An even better match between simulated and experimental band widths was obtained with FWHM = 0.095 eV (results not shown).

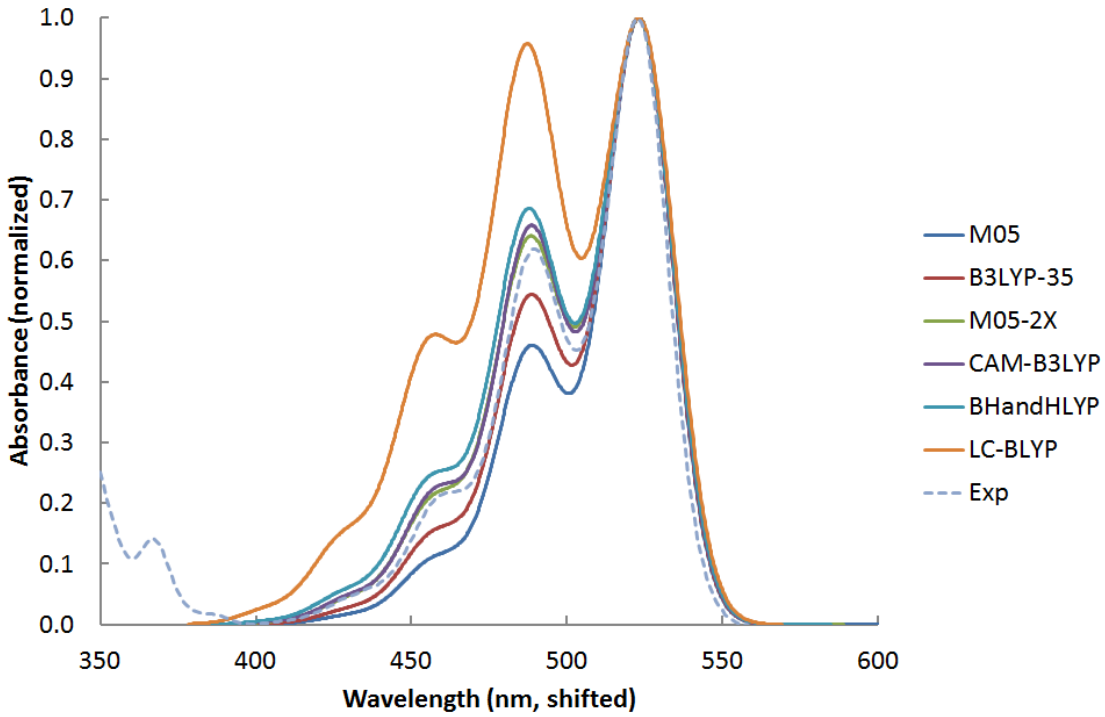


**Figure 2**. Visible absorption spectrum of PV19 as obtained with different XC functionals, the 6-31G(d) basis set and the IEFPCM (solvent = DMSO) in comparison with experiment after shifting the absorption maximum. The "geometry" method was used with "td" excited state geometries, no vibrational frequency scaling was used, and a FWHM of 0.1 eV was applied.

In order to allow a more detailed comparison between the spectra, the positions and relative intensities of the "0-1" band maxima are given in Table 4. All spectra were displaced in order to position the main maximum at exactly 523.0 nm. The position of the maximum of the "0-1" band is predicted with a less than 1 nm error relative to the experimental value with all functionals, except BHandHLYP and LC-BLYP. This suggests that no scaling of the vibrational frequencies is necessary with most of the functionals. Information about the

vibrational mode that is predominantly responsible for the band maxima in the vibronic structure (mode 71) is given in Section III.D. The energy difference between the "0-0" and "0-1"maxima is systematically slightly less than the energy of this mode, except when the two bands have similar intensity (i.e. the LC-BLYP result).

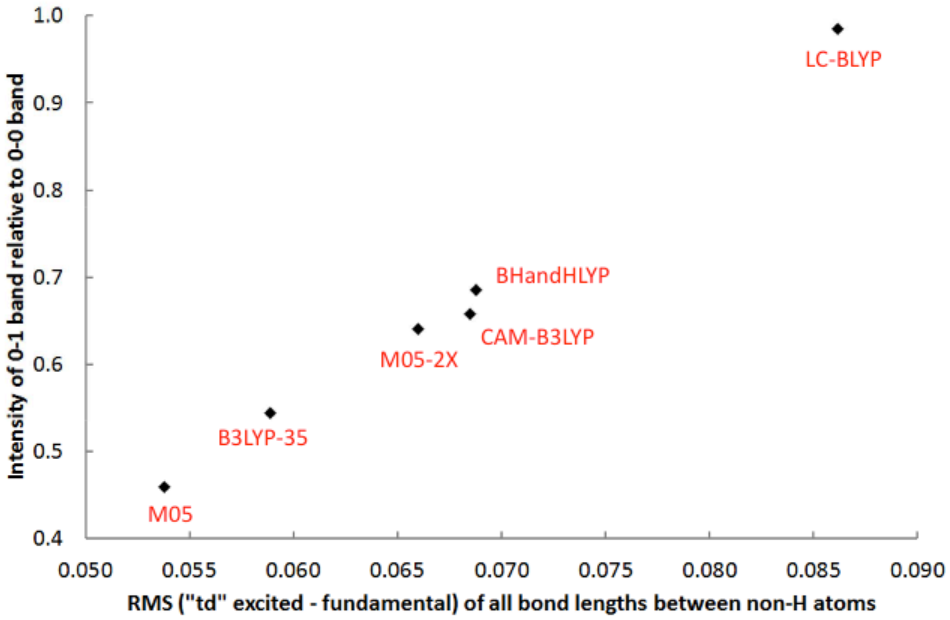


**Figure 3**. Relationship between the intensity of the 0-1 band relative to the 0-0 band and the RMS bond length displacement between the excited and fundamental state (in Å) for different XC functionals.

| | Relative intensity | Position (nm) | "0-1" – "0-0" Difference (eV) | Vibrational frequency (cm-1) | Vibrational energy (eV) |
|---|---|---|---|---|---|
| M05 | 0.460 | 488.8 | 0.166 | 1365.1 | 0.169 |
| B3LYP-35 | 0.544 | 488.6 | 0.167 | 1383.4 | 0.172 |
| M05-2X | 0.641 | 488.4 | 0.168 | 1386.5 | 0.172 |
| CAM-B3LYP | 0.658 | 488.6 | 0.167 | 1377.1 | 0.171 |
| BHandHLYP | 0.686 | 487.8 | 0.171 | 1411.8 | 0.175 |
| LC-BLYP | 0.958 | 487.2 | 0.174 | 1408.9 | 0.175 |
| Experiment | 0.619 | 489 | 0.165 | | |

**Table 4**. Positions and relative intensities of the "0-1" band with respect to the "0-0" band as determined with different XC functionals and the 6-31G(d) basis set in comparison to experiment. The vibrational frequency and corresponding vibrational energy of the predominant mode (mode 71) are also given. The "geometry" method was used with "td" excited state geometries, no vibrational frequency scaling was used, and a FWHM of 0.1 eV was applied.

The effect of the atomic basis set on the vibronic structure is now analyzed by comparing the 6-31G(d) results with those obtained with the 6-311G(d), 6-31+G(d), and 6-31+G(d,p) basis sets. All calculations were performed using the M05-2X XC functional, the "td" optimized excited state geometries, and the "geometry" method. The effect on the vibronic structure is relatively small, as shown in Fig. 4. Only the addition of triple-zeta functions results in a noticeable modification of the spectrum. This is consistent with Ref. 6d mentioning that the simple 6-31G basis set is close to providing a converged vibronic structure.

For a given functional and basis set, the differences in spectra generated with different methods are now illustrated. A first comparison, done with the M05-2X functional (Fig. 5), shows that the differences obtained by using the "td" versus the "eps" methods for optimization of the geometry of the excited state are small. This parameter turns out to be a rather unimportant one and, consequently, in most of the study it was decided to use mainly the "td" method.

After selecting the "td" method for the excited state geometry optimization, results obtained with the "duschinsky", "geometry" and "gradient" methods for simulating the spectrum are compared in Fig. 6 using the M05-2X XC functional. This comparison is possible in the case of PV19 because optimized geometries and vibrational frequencies of the excited state could be obtained. The three spectra are remarkably similar, as can also be judged from the data for the "0-1" band listed in Table 5. The line "Gaussian, no Duschinsky" refers to a calculation of the spectrum with the Gaussian package with Duschinsky rotation "switched off" by specifying "`jident`". This way of calculating the spectrum should closely correspond to the "geometry" method with our local code, as is indeed the case, since the only differences are the frequencies of the excited state that are calculated in Gaussian and set to those of the ground state in our code.

Remarkably, taking Duschinsky rotation of the vibrational modes into account or not has little impact. In order to better highlight possible Duschinsky effects spectra were simulated with a much smaller FWHM, producing a less blurred vibronic structure. Fig. 7 shows the spectra calculated with the "td" method, the M05-2X functional, and the Gaussian default HWHM of 135 $cm^{-1}$, equivalent to a FWHM of 0.0335 eV, with and without Duschinsky effects. Even with this 3 times better resolution the impact of Duschinsky rotation remains minimal and results mainly in a small displacement of the peak maxima.

Equally remarkably, the computationally significantly cheaper "gradient" method produces a spectrum that is very similar to the one that is obtained with the "geometry" method. Overall, the differences between the three methods are much smaller than the differences introduced by the choice of the functional, opening the way to rapid screening of the UV/vis absorption spectra of pigments and dyes, which behave like quinacridone. Indeed, if the electronic excitation was coupled to rotatable groups, the "gradient" and "geometry" methods would have led to different results and specific treatments should be employed.

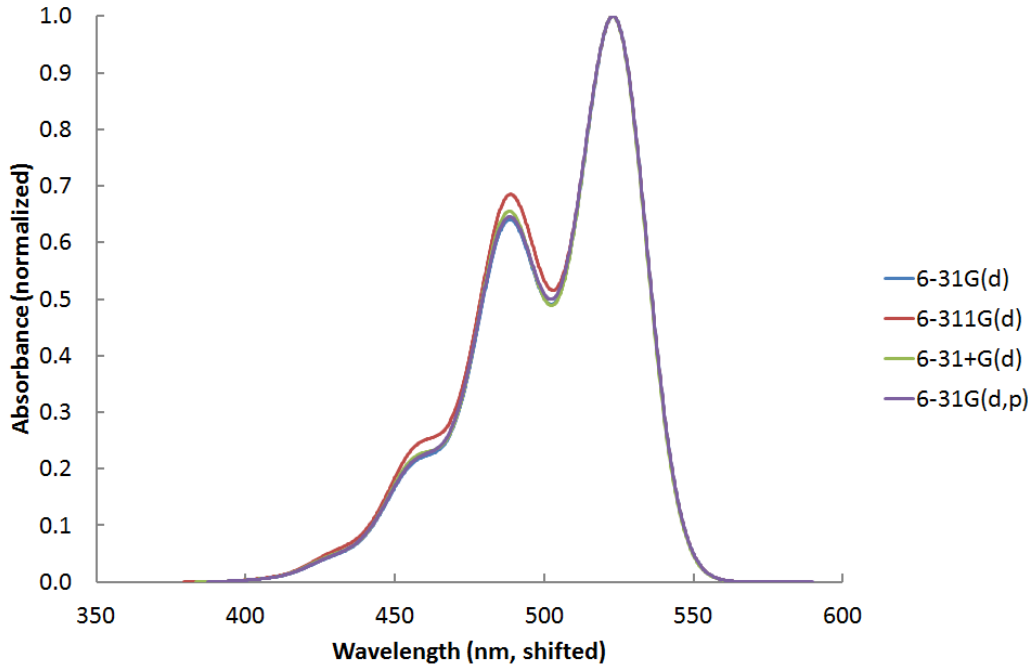


**Figure 4.** Comparison between the PV19 visible absorption spectra as obtained with different basis sets, the M05-2X XC functional, and IEFPCM (solvent = DMSO). The "geometry" method was used with "td" excited state geometries, no vibrational frequency scaling was used, and a FWHM of 0.1 eV was applied.

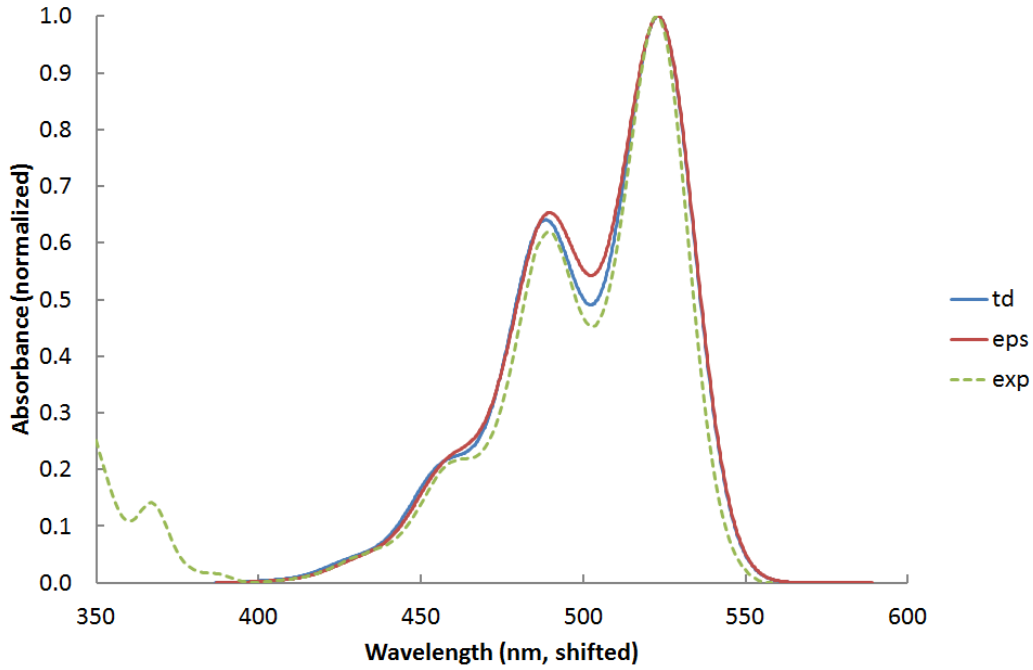


**Figure 5**. Comparison between the PV19 visible absorption spectra as obtained with M05-2X/6-31G(d) and the IEFPCM (DMSO) and the two methods for describing the non-equilibrium solvation effects in the excited state geometry optimization. The vibrational normal modes of both the ground and excited states were determined but no Duschinsky rotations were accounted for ("geometry" method). No vibrational frequency scaling was used and a FWHM of 0.1 eV was applied.

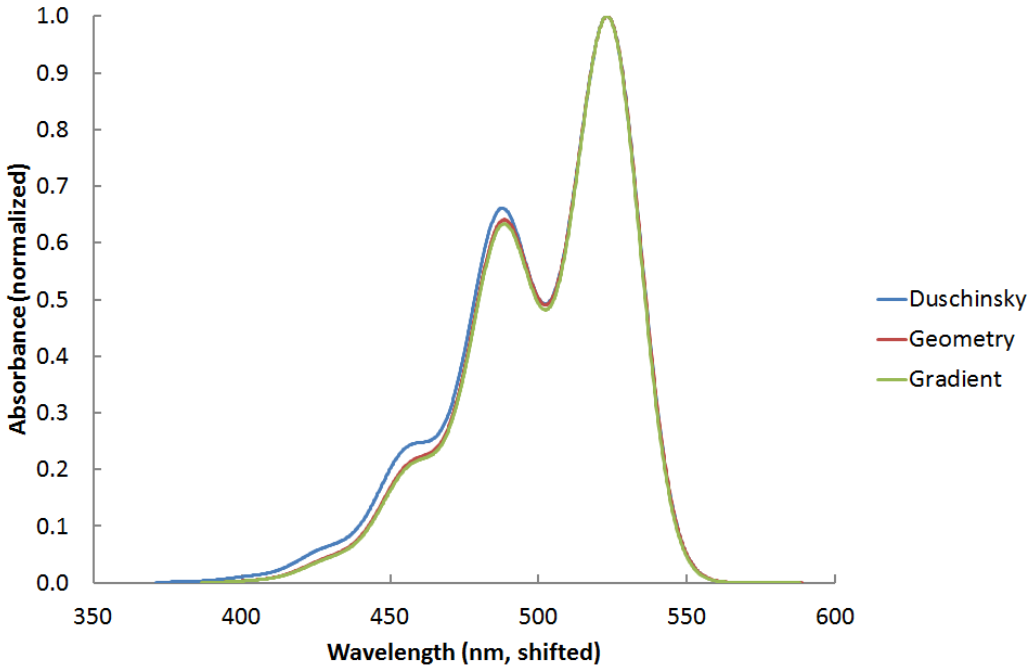


**Figure 6**. Comparison between the PV19 visible absorption spectra as obtained with M05-2X/6-31G(d) and the IEFPCM (DMSO) and three methods for simulating the vibronic structure. The excited state geometries were optimized with the "td" method, the vibrational frequencies were not scaled and a FWHM of 0.1 eV was applied.

| | Relative intensity | Position (nm) |
|---|---|---|
| Duschinsky | 0.661 | 487.7 |
| Gaussian, no Duschinsky | 0.650 | 488.7 |
| Geometry | 0.641 | 488.4 |
| Gradient | 0.633 | 488.4 |
| Experiment | 0.619 | 489 |

**Table 5**. Positions and relative intensities of the "0-1" band with respect to the "0-0" band as determined with different methods to simulate the vibronic structure in comparison to experiment. The "td" excited state geometries were obtained using M05-2X/6-31G(d) and the IEFPCM (solvent = DMSO) non-equilibrium solvation model. No vibrational frequency scaling was used, and a FWHM of 0.1 eV was applied.

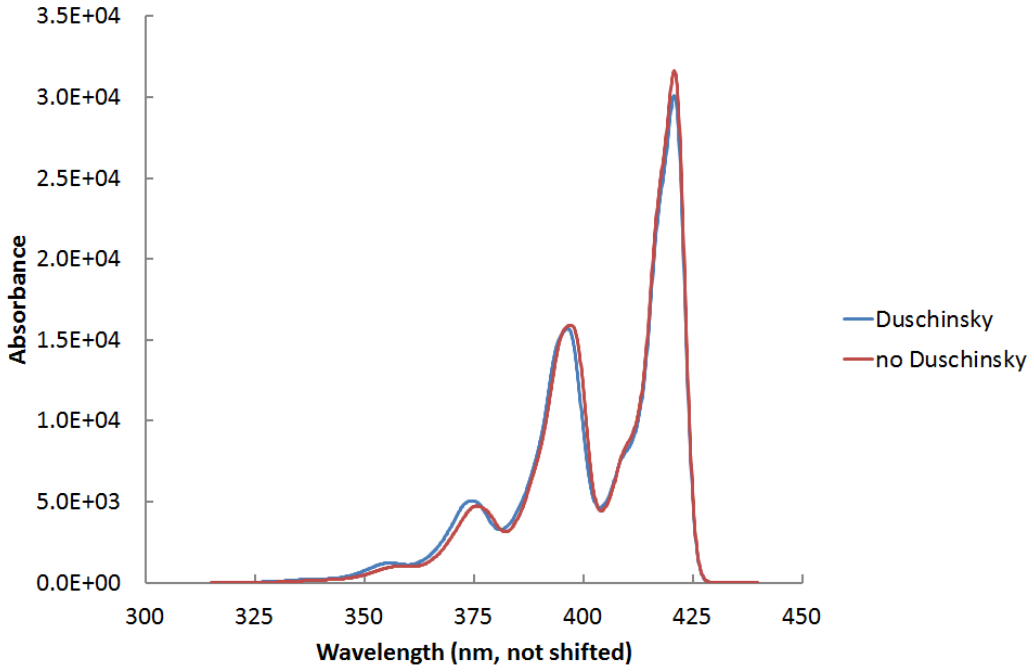


**Figure 7**. Impact of the Duschinsky rotation effects on the vibronic structure of the absorption spectrum of PV19 as obtained for a small FWHM of 0.0335 eV. The M05-2X XC functional was used in combination with the 6-31G(d) basis set, "td" method and IEFPCM (solvent = DMSO).

A plot of the Huang-Rhys factors obtained with the "geometry" and "gradient" methods illustrates why these two methods produce such a similar result (Fig. 8). Only the most relevant Huang-Rhys factors (> $1.10^{-6}$) are shown. There is a good correlation between HR factors obtained with the two methods, in particular for those modes with the largest HR factors. This illustrates the fact that the harmonic approximation and the displacement of the potential energy surface without frequency variations are indeed valid at the excited state since Eq. 1 is directly based on this approximation. Modes that couple only very weakly with the electronic excitation (HR factor < $1.10^{-6}$, not shown) show more difference between geometry- and gradient-derived HR factors, but such modes hardly influence the spectrum.

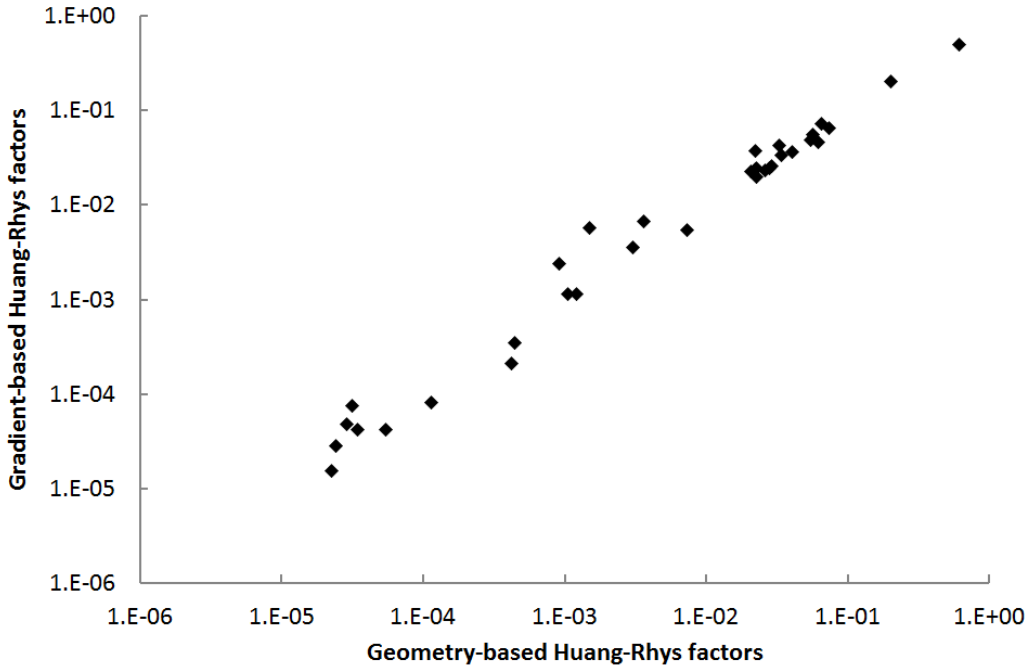


**Figure 8**. Comparisons between the Huang-Rhys factors obtained with the "geometry" and "gradient" methods. The M05-2X/6-31G(d) method was used in combination the "td" method and IEFPCM (solvent = DMSO). No vibrational frequency scaling was used.

As a final factor influencing the vibronic structure of the absorption spectrum, the effect of scaling the vibrational frequencies was studied. As shown already, frequency scaling might be necessary in cases where LC-BLYP or hybrid functionals with a high amount of HF exchange produce a vibronic structure intensity that best matches with the experimental spectrum. Indeed, in such cases the separation between the "0-0" and "0-1" bands is usually too large, due to an overestimation of the vibrational frequencies. Scaling the harmonic vibrational frequencies can however not be carried out independently since the Huang-Rhys factors ($HR_\ell$) and therefore the Franck-Condon factors [here $FC_\ell(\nu)$ is the Franck-Condon factor for a one-mode model with $\nu$ the vibrational quantum number] depend on the vibrational frequencies in the following way :

$$FC_\ell(\nu) = \frac{HR_\ell^{\nu} e^{-HR_\ell}}{\nu!} \tag{3}$$

where, within the "geometry" approach,

$$HR_\ell = \frac{1}{2}\frac{\omega_\ell}{\hbar}\left(\sum_{i,\alpha}\sqrt{m_i}\,Q_{i\alpha,\ell}\,\Delta X_{i\alpha}\right)^2 \tag{4}$$

whereas within the "gradient" approach,

$$HR_\ell = \frac{1}{2}\frac{1}{\hbar\omega_\ell^{\,3}}\left[\left(\frac{\partial E_e}{\partial Q_\ell}\right)_0\right]^2 \tag{5}$$

In Eq. 3, the sum runs over the i atoms and their α (x, y, and, z) coordinates, $m_i$ is the atomic mass, $Q_{i\alpha,\ell}$ is a component of the $\ell$ normal mode in the mass-weighted coordinates so that $\sum_{i,\alpha}\left(Q_{i\alpha,\ell}\right)^2 = 1$, and $\Delta X_{i\alpha}$, the difference of atomic coordinates upon excitation. Scaling the vibrational frequencies leads therefore to opposite modifications of the Huang-Rhys factors when applying the "geometry" and "gradient" approaches. The extent of these variations is illustrated by considering frequency scaling factors of 0.94 and 0.97. Spectra so obtained are compared with the spectrum simulated without frequency scaling (Figure 9). The frequency-scaled geometry-based spectrum has a less intense vibronic structure, because all Huang-Rhys factors have been multiplied by 0.94 or 0.97. The frequency-scaled gradient-based spectrum, on the other hand, has a more intense vibronic structure, because all Huang-Rhys factors have been multiplied by $1/(0.94)^3 = 1.2040$ or $1/(0.97)^3 = 1.0957$.

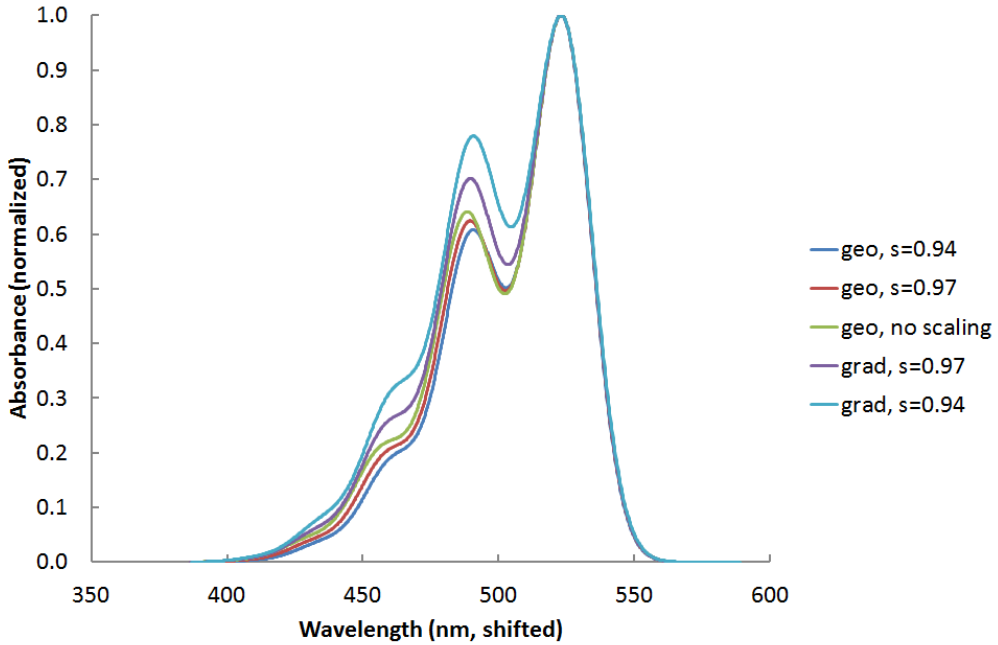


**Figure 9**. Impact of the vibrational frequency scaling on the PV19 visible absorption spectra as obtained with M05-2X/6-31G(d) and the IEFPCM (DMSO) and two methods for simulating the vibronic structure. The excited state geometries were optimized with the "td" non-equilibrium solvation model. A FWHM of 0.1 eV was applied.

### *III.D. Main vibrational normal modes and excited state geometries*

Fig. 10 sketches the Huang-Rhys factors for the vibrational modes to reveal which modes couple most strongly to the electronic excitation and are therefore mostly responsible for the vibronic structure. The modes have been numbered in order of increasing frequency. The Huang-Rhys factors shown here were calculated using M05-2X/6-31G(d) and the "td/geometry" method without scaling of the vibrational frequencies. PV19 has 102 vibrational normal modes. All modes were included in the calculation of the spectrum, given

the fact that there are no low-frequency modes with very high HR factor. The modes with the highest Huang-Rhys factor are mode 9 (HR factor = 0.607, 235.5 $cm^{-1}$ or 0.0292 eV) and mode 71 (HR factor = 0.201, 1386.5 $cm^{-1}$ or 0.172 eV). Their impact can easily be seen on Fig. 11, which displays a stick spectrum together with the peak-broadened result. Five peaks in the stick spectrum have been labeled. The most intense one is due to the 0-0 excitation, while the other four have been labeled according to the vibrational mode(s) that is/are excited (main number) and the number of vibrational quanta in the mode(s) (subscript). Mode 71 is responsible for the most dominant and noticeable vibronic progression in the spectrum. Indeed, as already mentioned, the 0.165 eV separation between the "0-0" and "0-1" band maxima in the experimental spectrum matches well the vibrational energy of mode 71 (0.172 eV). In addition, mode 9 produces the most intense progression within each band (notice the 3 most intense transitions under the "0-0" band labeled "523". This spectrum is the result of 6349 vibronic excitations, resulting in a sum of Franck-Condon factors of 0.993. Simulations with the other functionals and other methods produce very similar results in terms of predominant modes, number of relevant vibrational excitations, and sum of Franck-Condon factors.

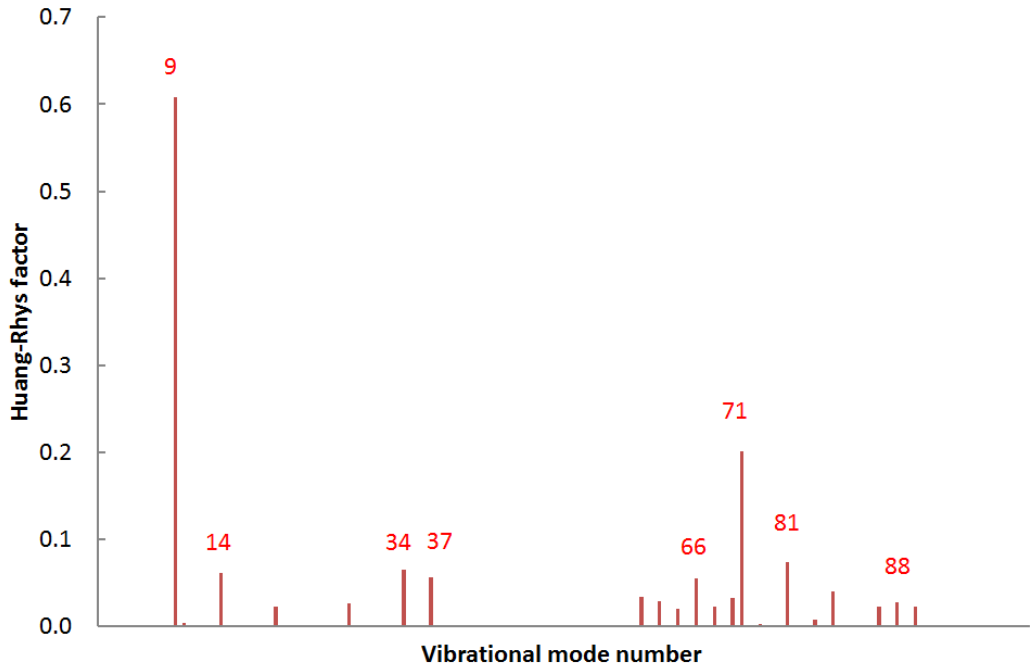


**Figure 10**. Huang-Rhys factors for PV19 as determined with M05-2X/6-31G(d) and the "td/geometry" method, without scaling of the vibrational frequencies.

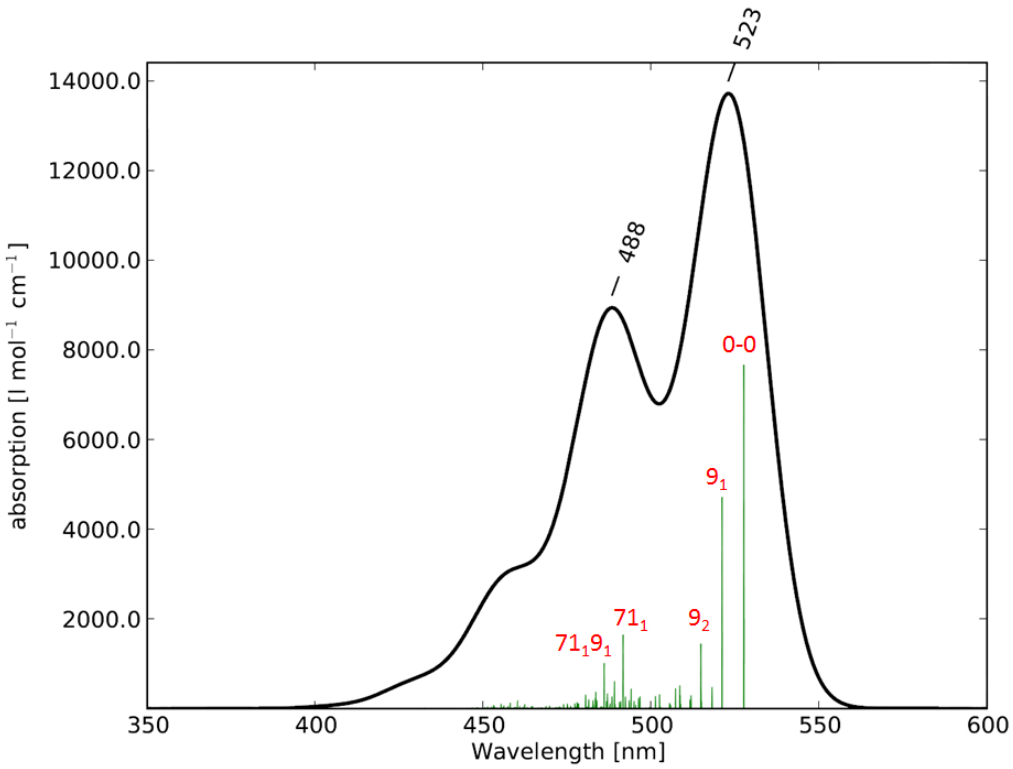


**Figure 11**. Absorption spectrum of PV19 as determined with M05-2X/6-31G(d) and the "td/geometry" method without scaling of the vibrational frequencies, and its decomposition in terms of the dominant FC factors.

In order to understand the reason for the predominance of these two modes they can be visualized and their nuclear displacements can be compared with the differences between the ground state and excited state equilibrium geometries. Given the absence of rotatable bonds, both the ground state and the excited state have a perfectly planar geometry at equilibrium and belong to the $C_{2h}$ point group. The equilibrium bond lengths are given in Table 6 (results again with M05-2X/6-31G(d)) together with the differences of bond lengths upon excitation. In Fig. 12, the bond length variations upon excitation are displayed whereas Fig. 13 sketches the atomic displacements of vibrational modes 9 and 71, which present the largest HR factors. The strong coupling between mode 9 and the electronic excitation originates from the ensemble motion of the carbon skeleton, which is twisted while the H atoms follow the C atoms on which they are linked. In the case of mode 71, the coupling is even more obvious and corresponds to the lengthening of bonds 2, 6, 8, and 9 while bonds 3, 5, and 10 are shortening. This corresponds to the excitation-induced transition from a more quinonoid-like structure to a more aromatic- or phenolate-like one (Fig. 13).

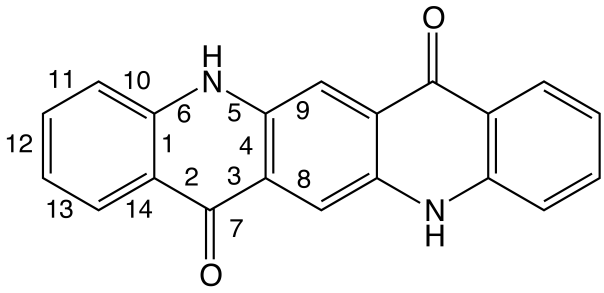


| Bond # | Ground state | Excited state | Difference |
|---|---|---|---|
| 1 | 1.4082 | 1.4082 | 0.0000 |
| 2 | 1.4646 | 1.4768 | 0.0122 |
| 3 | 1.4775 | 1.4483 | -0.0292 |
| 4 | 1.4137 | 1.4293 | 0.0156 |
| 5 | 1.3761 | 1.3562 | -0.0199 |
| 6 | 1.3691 | 1.3838 | 0.0147 |
| 7 | 1.2302 | 1.2426 | 0.0124 |
| 8 | 1.3898 | 1.3981 | 0.0083 |
| 9 | 1.3928 | 1.4026 | 0.0098 |
| 10 | 1.4086 | 1.3970 | -0.0116 |
| 11 | 1.3786 | 1.3908 | 0.0122 |
| 12 | 1.4069 | 1.3955 | -0.0114 |
| 13 | 1.3776 | 1.3924 | 0.0148 |
| 14 | 1.4057 | 1.3935 | -0.0122 |

**Table 6**. Representative optimized bond lengths (Å) of the ground and excited states, as well as their differences, calculated with the M05-2X XC functional, the 6-31G(d) basis set, the "td" non-equilibrium method and IEFPCM. Only the symmetry non-equivalent bond lengths are given.

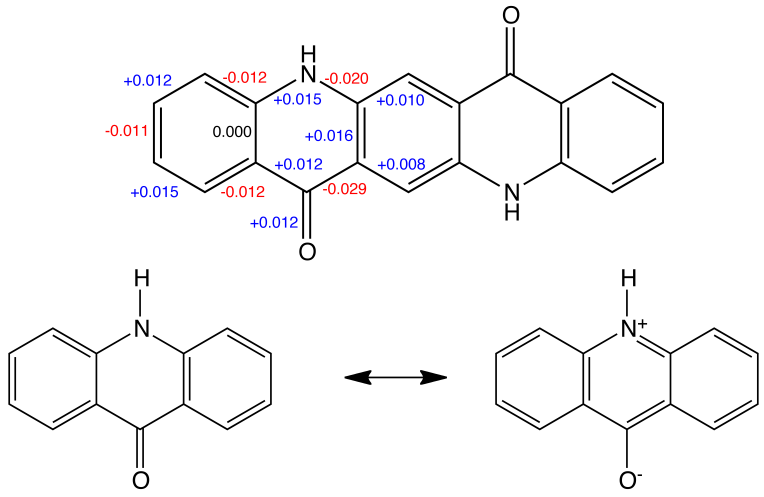


**Figure 12**. Variations of the optimized bond lengths (Å) from the ground to the excited state of PV19 (top), as calculated with the M05-2X XC functional and the IEFPCM method and sketch of the quinonoid-to-aromatic transition (bottom).

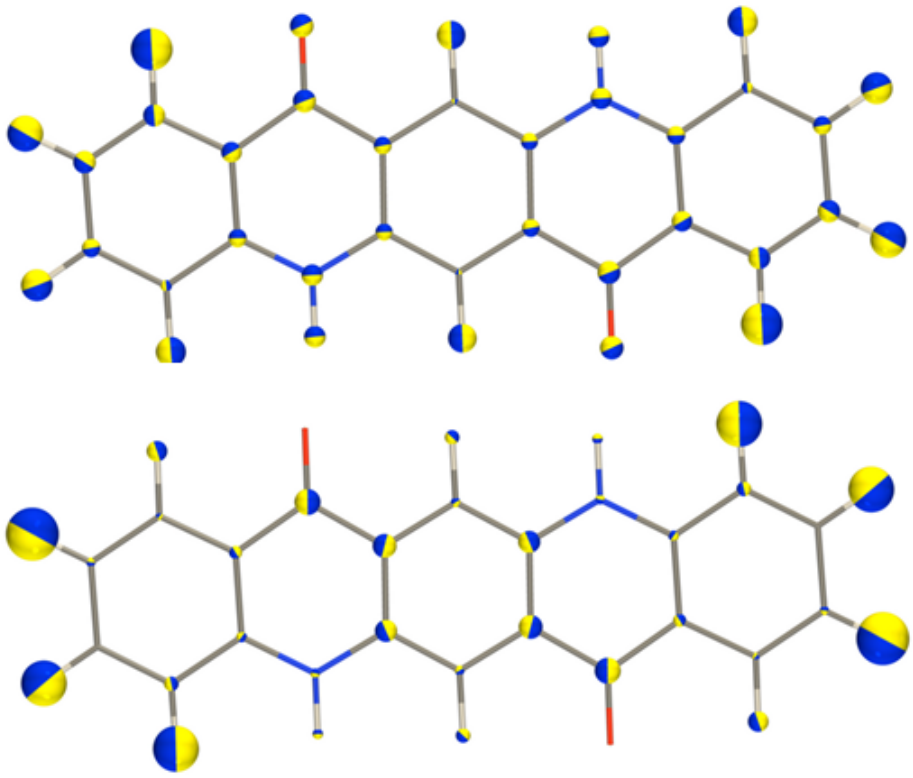

**Figure 13**. PyVib2[24] sketches of the atomic displacements of the vibrational normal modes 9 (top) and 71 (bottom). The direction of atomic displacements is perpendicular to the junction plane between the two hemispheres of distinct color, and their amplitudes are proportional to the radius of the sphere. The sum of the surfaces of the spheres is always constant.

## IV. Conclusions

PV19, a typical quinacridone pigment has been used to analyze the impact of several parameters on the UV/vis absorption band shape in solution, simulated using density functional theory and time-dependent density functional theory levels of approximation. These encompass, i) the choice of exchange-correlation functional, ii) the basis set, iii) the method for non-equilibrium geometry optimization of the excited state, iv) the approach for evaluating the vibronic band structure, v) the peak broadening, and vi) the scaling of the harmonic vibrational frequencies.

First, the equilibrium solvation geometry optimization method where the static dielectric constant is replaced by the dynamic dielectric constant, effectively causing only the electronic degrees of freedom of the solvent to adapt to the modified electron density of the excited state provides very similar spectra as the standard Gaussian non-equilibrium geometry optimization technique. Then, the "Duschinsky", "geometry", and "gradient" methods provide very similar vibronic structures. The first, accounting for Duschinsky

rotation, is the most costly because it requires the evaluation of the geometry and vibrational frequencies of the excited state. In the "geometry" method, the excited state geometry is optimized whereas in the "gradient" method, only one step of geometry optimization is carried out and the gradients are used to evaluate the Huang-Rhys factors as well as to determine the excited state geometries. Remarkably, the "gradient" method, computationally significantly cheaper, produces a spectrum that is very similar to the other ones obtained with the "Duschinsky" and "geometry" methods, opening the way to a fast simulation of the UV/vis absorption spectra of pigments and dyes, which behave like quinacridone, i.e. where there is no coupling between the electronic excitation on the skeleton and rotatable substituents. Scaling the calculated vibrational frequencies to account for anharmonicity effects as well as for limitation of the method also impacts the shape of the vibronic spectrum and this effect depends on the method used to determine the Huang-Rhys factors. Indeed, scaling the vibrational frequencies – by a factor which is typically smaller than 1.0 and larger than 0.92 with most XC functionals – results in a relative decrease of the 0-1 peak intensity with respect to the 0-0 band when optimizing the geometry of the excited state whereas the effect is opposite and magnified if using the gradient method. Though these different parameters together with the broadening effects have an impact on the vibronic structure and lead to different levels of agreement with experiment, the choice of exchange-correlation functional is certainly of the most importance because it can drastically modify the spectral shape. In the case of PV19, the M05-2X and to a lesser extent CAM-B3LYP XC functionals are the most efficient to reproduce the vibronic structure, confirming the important role of exact Hartree-Fock exchange. Still, these functionals are not the most reliable to predict the excitation energies and oscillator strengths, and particularly the energies of maximum absorption intensities. Indeed, a functional with less HF exchange, like M05, performs better with overestimations of the order of 0.25 eV, with respect to M05-2X and its 0.58 eV overestimation. The M05 functional is also the one that gives an oscillator strength closest to the experimental value.

## Acknowledgments

V.L. thanks the F.R.S.-FNRS for his Research Associate position. This work has been supported by the Academy Louvain (ARC "Extended π-Conjugated Molecular Tinkertoys for Optoelectronics, and Spintronics") and by the Belgian Government (IUAP N° P7-05 "Functional Supramolecular Systems"). The calculations were performed on the computing facilities of the Consortium des Équipements de Calcul Intensif (CÉCI), in particular those of the Plateforme Technologique de Calcul Intensif (PTCI) installed in the University of Namur, for which we gratefully acknowledge financial support of the FNRS-FRFC (Conventions No. 2.4.617.07.F and 2.5020.11).

## Bibliography


1 R. J. D. Tilley, Colour and the Optical Properties of Materials, John Wiley & Sons, Chichester, 2000.

2 R. M. Christie, Colour Chemistry, RSC, Cambridge, 2001.

3 (a) B. Mennucci, Modeling environment effects on spectroscopies through QM/classical models, *Phys. Chem. Chem. Phys.*, 2013, **15**, 6583-6594; (b) C. Adamo and D. Jacquemin, The calculations of excited-state properties with Time-Dependent Density Functional Theory, *Chem. Soc. Rev.*, 2013, **42**, 845-856; (c) C. Faber, P. Boulanger, C. Attaccalite, I. Duchemin and X. Blase, Excited states properties of organic molecules: from density functional theory to the GW and Bethe-Salpeter Green's function formalisms, *Phil. Trans. R. Soc.*, 2014, **A372**, 20130271; (d) V. Barone, M. Biczysko, J. Bloino, L. Carta and A. Pedone, Environmental and dynamical effects on the optical properties of molecular systems by time-independent and time-dependent approaches. Coumarin derivatives as test cases, *Comput. Theor. Chem.*, 2014, **1037**, 35-48.

4 (a) M. Schreiber, M. R. Silva-Junior, S. P. A. Sauer and W. Thiel, Benchmarks for electronically excited states: CASPT2, CC2, CCSD, and CC3, *J. Chem. Phys.*, 2008, **128**, 134110; (b) R. Send, V. R. I. Kaila and D. Sundholm, Reduction of the virtual space for coupled-cluster excitation energies of large molecules and embedded systems, *J. Chem. Phys.*, 2011, **134**, 214114; (c) C. Faber, I. Duchemin, T. Deutsch and X. Blase, Many-body Green's function study of coumarins for dye-sensitized solar cells, *Phys. Rev. B,* 2012, **86**, 155315; (d) Y. A. Bernard, Y. Shao and A. I. Krylov, General formulation of spin-flip time-dependent density functional theory using non-collinear kernels: Theory, implementation, and benchmarks, *J. Chem. Phys.*, 2012, **136**, 204103; (e) N. O. C. Winter, N. K. Graf, S. Leutwyler and C. Hättig, Benchmarks for 0-0 transitions of aromatic organic molecules: DFT/B3LYP, ADC(2), CC2, SOS-CC2 and SCS-CC2 compared to high-resolution gas-phase data, *Phys. Chem. Chem. Phys.*, 2013, **15**, 6623-6630; (f) R. Fukuda and M. Ehara, Electronic excited states and electronic spectra of biphenyl: a study using many-body wavefunction methods and density functional theories, *Phys. Chem. Chem. Phys.*, 2013, **15**, 17426-17434; (g) X. Liu, Q. Ou, E. Alguire and J. E. Subotnik, An inexpensive, variational, almost black-box, almost size-consistent correction to configuration interaction singles for valence excited states, *J. Chem. Phys.*, 2013, **138**, 221105; (h) E. Walczak, B. Szefczyk and T. Andruniow, Geometries and Vertical Excitation Energies in Retinal Analogues Resolved at the CASPT2 Level of Theory: Critical Assessment of the Performance of CASSCF, CC2, and DFT Methods, *J. Chem. Theor. Comput.*, 2013, **9**, 4915-4927; (i) S. Knecht, C. M. Marian, J. Kongsted and B. Mennucci, On the Photophysics of Carotenoids: A Multireference DFT Study of Peridinin, *J. Phys. Chem. B*, 2013, **117**, 13808-13815; (j) O. Valsson, P. Campomanes, I. Tavernelli, U. Rothlisberger and C. Filippi, Rhodopsin Absorption from First Principles: Bypassing Common Pitfalls, *J. Chem. Theor. Comput.*, 2013, **9**, 2441-2454; (k) E. Ronca, C. Angeli, L. Belpassi, F. De Angelis, F.

Tarantelli and M. Pastore, Density Relaxation in Time-Dependent Density Functional Theory: Combining Relaxed Density Natural Orbitals and Multireference Perturbation Theories for an Improved Description of Excited states, *J. Chem. Theor. Comput.*, 2014, **10**, 4014-4024.

5 (a) A. Kovyrshin, F. De Angelis and J. Neugebauer, Selective TDDFT with automatic removal of ghost transitions: application to a perylene-dye-sensitized solar cell model, *Phys. Chem. Chem. Phys.*, 2012, **14**, 8608-8619; (b) S. S. Leang, F. Zahariev and M. S. Gordon, Benchmarking the performance of time-dependent density functional methods, *J. Chem. Phys.*, 2012, **136**, 104101; (c) T. Petrenko and F. Neese, Efficient and automatic calculation of optical band shapes and resonance Raman spectra for larger molecules within the independent mode displaced harmonic oscillator model, *J. Chem. Phys.*, 2012, **137**, 234107; (d) G. V. Lopez, C. H. Chang, P. M. Johnson, G. E. Hall, T. J. Sears, B. Markiewicz, M. Milan and A. Teslja, What is the Best DFT Functional for Vibronic Calculations? A Comparison of the Calculated Vibronic Structure of the S1-S0 Transition of Phenylacetylene with Cavity Ringdown Band Intensities, *J. Phys. Chem. A*, 2012, **116**, 6750-6758; (e) B. Moore II and J. Autschbach, Longest-Wavelength Electronic Excitations of Linear Cyanines: The Role of Electron Delocalization and of Approximations in Time-Dependent Density Functional Theory, *J. Chem. Theor. Comput.*, 2013, **9**, 4991-5003.

6 (a) S. Agrawal, P. Dev, N. J. English, K. Ravindranathan Thampi and J. M. D. MacElroy, A TD-DFT study of the effects of structural variations on the photochemistry of polyene dyes, *Chem. Sci.*, 2012, **3**, 416-424; (b) S. Höfener, P. C. Kooijman, J. Groen, F. Ariese and L. Visscher, Fluorescence behavior of (selected) flavonols: a combined experimental and computational study, *Phys. Chem. Chem. Phys.,* 2013, **15**, 12572-12581; (c) D. Jacquemin, A. Planchat, C. Adamo and B. Mennucci, TD-DFT Assessment of Functionals for Optical 0-0 Transitions in Solvated Dyes, *J. Chem. Theor. Comput.*, 2012, **8**, 2359-2372; (d) A. Charaf-Eddin, A. Planchat, B. Mennucci, C. Adamo and D. Jacquemin, Choosing a Functional for Computing Absorption and Fluorescence Band Shapes with TD-DFT, *J. Chem. Theor. Comput.*, 2013, **9**, 2749-2760; (e) A. Graczyk, J. M. Zurek and M. J. Paterson, On the linear and non-linear electronic spectroscopy of chlorophylls: a computational study, *Photochem. Photobiol. Sci.*, 2014, **13**, 103-111.

7 (a) J. Mizuguchi and T. Senju, Solution and solid-state spectra of quinacridone derivatives as viewed from the intermolecular hydrogen bond, *J. Phys. Chem. B,* 2006, **110**, 19154-19161; (b) T. Senju, N. Nishimura and J. Mizuguchi, Polymorph of 2,9-Dichloroquinacridone and its Electronic Properties, *J. Phys. Chem. A,* 2007, **111**, 2966-2970; (c) T. Senju and J. Mizuguchi, The electronic structure of C.I. Pigment Red 209, *Dyes and Pigments,* 2008, **76**, 760-764; (d) H. Fukunaga, D. G. Fedorov, M. Chiba, K. Nii and K. Kitaura, Theoretical analysis of the intermolecular interaction effects on the

excitation energy of organic pigments: solid-state quinacridone, *J. Phys. Chem. A,* 2008, **112**, 10887-10894.

8 J. Tomasi, B. Mennucci and R. Cammi, Quantum Mechanical Continuum Solvation Models, *Chem. Rev.,* 2005, **105**, 2999-3093.

9 (a) J. Guthmuller and B. Champagne, Time dependent density functional theory investigation of the resonance Raman properties of the julolidinemalononitrile push-pull chromophore in various solvents, *J. Chem. Phys.,* 2007, **127**, 164507; (b) J. Guthmuller, B. Champagne, C. Moucheron and A. Kirsch-De Mesmaeker, Investigation of the Resonance Raman Spectra and Excitation Profiles of a Monometallic Ruthenium(II) [Ru(bpy)2(HAT)]2+ Complex by Time-Dependent Density Functional Theory, *J. Phys. Chem. B*, 2010, **114**, 511-520.

10 M. J. Frisch *et al.*, Gaussian 92/DFT, Revision F.2; Gaussian, Inc.: Pittsburgh PA, 1993.

11 Y. Zhao, N. E. Schultz and D. G. Truhlar, Design of Density Functionals by Combining the Method of Constraint Satisfaction with Parametrization for Thermochemistry, Thermochemical Kinetics, and Noncovalent Interactions, *J. Chem. Theory Comput*., 2006, **2**, 364-382.

12 H. Iikura, T. Tsuneda, T. Yanai and K. Hirao, A long-range correction scheme for generalized-gradient-approximation exchange functionals, *J. Chem. Phys*. 2001, **115**, 3540-3544.

13 T. Yanai, D. P. Tew and N. C. Handy, A new hybrid exchange-correlation functional using the Coulomb-attenuating method (CAM-B3LYP), *Chem. Phys. Lett.*, 2004, **393**, 51-57.

14 A. D. Becke, Density-functional thermochemistry. III. The role of exact exchange, *J. Chem. Phys.*, 1993, **98**, 5648-5652.

15 Y. Zhao and D. G. Truhlar, The MO6 suite of density functionals for main group thermochemistry, thermochemical kinetics, noncovalent interactions, excited states, and transition elements: two new functionals and systematic testing of four MO6-class functionals and 12 other functionals, *Theor. Chem. Acc*., 2008, **120**, 215-241.

16 Gaussian 09 (Revisions A.02 and C.02) M.J. Frisch *et al.* Gaussian, Inc., Wallingford CT, 2009.

17 (a) E. Runge and E. K. U. Gross, Density-functional theory for time-dependent systems, *Phys. Rev. Lett.*, 1984, **52**, 997-1000; (b) M. E. Casida in *Time-Dependent Density-Functional Response Theory for Molecules,* ed. D. P. Chong, World Scientific, Singapore, 1995, vol. **1**, pp. 155-192; (c) *Fundamentals of Time-Dependent Density Functional Theory*, ed. M. A. L. Marques, F. M. S. Nogueira, E. K. U. Gross and A. Rubio, Springer-Verlag, Heidelberg, 2012, vol. **837**.

18 (a) F. Furche and R. Ahlrichs, Adiabatic time-dependent density functional methods for excited state properties, *J. Chem. Phys.*, 2002, **117**, 7433-7447; (b) G. Scalmani, M. J. Frisch, B. Mennucci, J. Tomasi, R. Cammi and V. Barone, Geometries and properties of excited states in the gas phase and in solution: theory and application of a time-dependent density functional theory polarizable continuum model, *J. Chem. Phys.*, 2006, **124**, 094107.

19 M. Cossi and V. Barone, Time-dependent density functional theory for molecules in liquid solutions, *J. Chem. Phys.*, 2001, **115**, 4708-4717.

20 (a) F. Duschinskii, *Acta Physicochem. URSS*, 1937, **7**, 551; (b) R. Berger, C. Fischer and M. Klessinger, Calculation of the Vibronic Fine Structure in Electronic Spectra at Higher Temperatures. 1 . Benzene and Pyrazine, *J. Phys. Chem. A*, 1998, **102**, 7157-7167; (c) M. Dierksen and S. Grimme, Density functional calculations of the vibronic structure of electronic absorption spectra, *J. Chem. Phys.*, 2004, **120**, 3544-3554.

21 (a) F. J. A. Ferrer, V. Barone, C. Cappelli and F. Santoro, Duschinsky, Herzberg-Teller, and Multiple Electronic Resonance Interferential Effects in Resonance Raman Spectra and Excitation Profiles. The Case of Pyrene, *J. Chem. Theor. Comput.*, 2013, **9**, 3597-3611; (b) V. Barone, J. Bloino, M. Biczysko and F. Santoro, Fully Integrated Approach to Compute Vibrationally Resolved Optical Spectra: From Small Molecules to Macrosystems, *J. Chem. Theory Comput.*, 2009, **5**, 540-554.

22 J. P. Merrick, D. Moran and L. Radom, An evaluation of Harmonic Vibrational Frequency Scale Factors, *J. Phys. Chem. A*, 2007, **111**, 11683-11700.

23 (a) M. Miura, Y. Aoki and B. Champagne, Assessment of time-dependent density functional schemes for computing the oscillator strengths of benzene, phenol, aniline, and fluorobenzene, *J. Chem. Phys.*, 2007, **127**, 084103; (b), M. Caricato, G. W. Trucks, M. J. Frisch and K. B. Wiberg, Oscillator Strength: How Does TDDFT Compare to EOM-CCSD?, *J. Chem. Theor. Comput.*, 2011, **7**, 456-466.

24 (a) M. Fedorovsky, PyVib2, A Program for Analyzing Vibrational Motion and Vibrational Spectra, 2007, http://pyvib2.sourceforge.net; (b) M. Fedorovsky, Exploring vibrational optical activity with PyVib2, *Comput. Lett.*, 2006, **2**, 233; (c) V. Liégeois and B. Champagne, Implementation in the Pyvib2 program of the localized mode method and application to a helicene, *Theor. Chem. Acc.*, 2012, **131**, 1284, 1-15.